GOLD EMBRITTLEMENT IN LEADFREE SOLDER

Craig Hillman, Nathan Blattau, Joelle Arnold, Thomas Johnston, Stephanie Gulbrandsen
DfR Solutions
Beltsville, MD, USA
chillman@dfrsolutions.com

Julie Silk
Agilent Technologies
Santa Rosa, CA

Alex Chiu
Agilent Technologies
Penang, Malaysia

ABSTRACT

Gold embrittlement in SnPb solder is a well-known failure mechanism in electronic assembly. To avoid this issue, prior studies have indicated a maximum gold content of three weight percent. This study attempts to provide similar guidance for Pb-free (SAC305) solder. Standard surface mount devices were assembled with SnPb and SAC305 solder onto printed boards with various thicknesses of gold plating. The gold plating included electroless nickel immersion gold (ENIG) and electrolytic gold of 15, 25, 35, and 50 microinches over nickel. These gold thicknesses resulted in weight percentages between 0.4 to 7.0 weight percent.

Samples were aged for up to 1000 hours and then subjected to a range of environmental stresses, including thermal cycling, and both low and high speed shear testing. Results from thermal cycling indicated an elevated risk of early life failures in SnPb solder joints once gold weight percentage exceeds four percent, which is in line with the results from previous studies. SAC solder showed no indication of early life failures during temperature cycling, yet showed progressive degradation with increasing Au content.

The results from low and high speed shear testing seem to suggest that SAC305 solder is more capable of maintaining mechanical properties with increasing gold content. This improvement in gold embrittlement may be partially explained by the additional tin content. Fractography was performed to confirm transitions from ductile to brittle behavior. Metallographic inspections and x-ray mapping were performed to confirm calculated gold content and assess the influence of intermetallic morphology and location on mechanical performance.

Key words: SAC solder, gold embrittlement, high speed shear testing, thermal cycling, intermetallic

INTRODUCTION

Gold embrittlement of solder has been a concern for electronic manufacturers since the early days of electronics, with the generally accepted first articles on the topic published in 1963 by Foster [1] and Harding and Pressley [2]. Foster wrote of a noticeable drop in elongation and a transition from ductile to brittle fracture between 5 weight percent and 10 weight percent gold in 60-40 SnPb solder. However, in regards to shear strength, the decreases were more gradual, with only a 20% decrease even up to 15 weight percent gold.

Harding and Pressley also observed similar phenomenon. Their publication defined the critical amount to avoid embrittlement as based on gold thickness. While the authors recommended thicknesses less than 50 microinches (1.25 microns) to avoid 'measurable detrimental effects', they noted that the strength reduction was inverse to the gold content. This would seem, as with Foster, to indicate a progressive reduction with no abrupt change in mechanical properties.

Further work by Bester [3] and Wild [4] further narrowed a critical gold content in SnPb solder to somewhere above 4 to 5 weight percent. More recent investigations by Glazer [5] and Banks [6], focused on long-term reliability, reduced the critical gold content down to 3 weight percent, where it has become the accepted norm in the electronics industry, especially in high reliability applications.

This 'line-in-the-sand' has been helpful in providing quality/manufacturing/reliability engineers clear go/no-go decision points regarding the acceptability of SnPb solder joints assembled to either components or printed circuit boards with a thick gold coating. But the transition to RoHS compliant product has driven SAC305 as the default solder of choice in electronics assembly. While several papers [7-10] have studied gold embrittlement in SAC305 solder, none have been able to provide a similar demarcation with regard to an acceptable level of gold content.

In an attempt to identify the appropriate level of gold content in SAC305, the authors have used tests to characterize strength, ductility, and long-term reliability of SAC305 solder joints with a wide range of weight percent gold. For each test, samples were aged for varying lengths of time to capture long-term diffusion and reaction mechanisms that could decrease the robustness of the SAC305 solder.

TEST SAMPLES
Test samples consisted of 2512 and 1206 ceramic chip resistors assembled to printed circuit boards with varying thicknesses of gold plating. A schematic of the test coupon is shown in Figure 1.
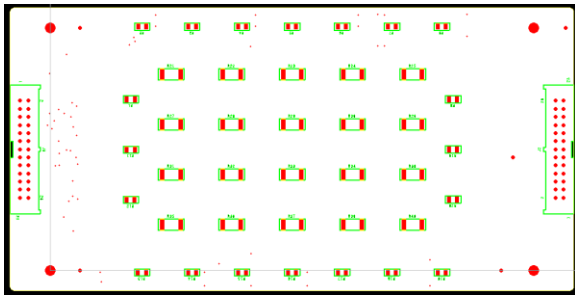
Figure 1: Test coupon

The specified plated gold thickness and stencil thickness were varied to create solder joints with a range of gold content. Details on the experimental design are provided in Table 1.

Table 1: Experimental Design

Number of Boards	Stencil Thickness	Gold Plating	Gold Thickness	Solder
15	4 Mil	Electrolytic	50 µin	SAC
15	4 Mil	Electrolytic	50 µin	SnPb
15	5 Mil	Electrolytic	35 µin	SAC
15	5 Mil	Electrolytic	35 µin	SnPb
15	5 Mil	Electrolytic	25 µin	SAC
16	N/A	Electrolytic	15 µin	SAC
16	N/A	ENIG	< 5 µin	SAC

Gold Content Calculations
The actual thickness of the gold plating was measured at six points on the board using Xray Fluorescence (XRF). The locations of three measurement points are displayed in Figure 2. The averages for the six test points across all the samples are shown in Table 2.
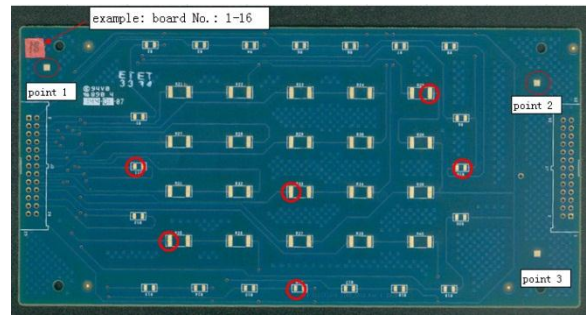

Figure 2: Gold thickness measurements

Table 2: Gold thickness measurements

Board Type	Quantity	Average	Minimum	Maximum
		µinches		
ENIG	16	3.6	3.0	4.2
15 µin	16	20.6	18.9	22.1
25 µin	30	30.0	26.7	35.0
35 µin	30	45.6	38.6	49.1
50 µin	30	56.5	50.7	63.2

To accurately capture actual gold content in the solder, three dimensional (3D) solder paste measurement was performed on all of the assemblies prior to reflow. The measured solder paste volume deposited on the pads after stencil print is displayed in Figure 3 for bond pads under the 1206 component and Figure 4 for bond pads under the 2512 component.
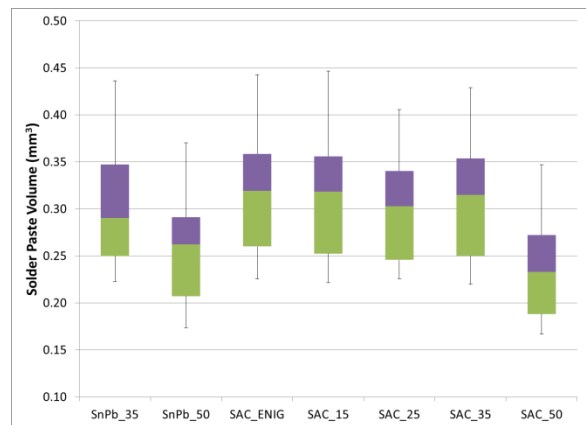

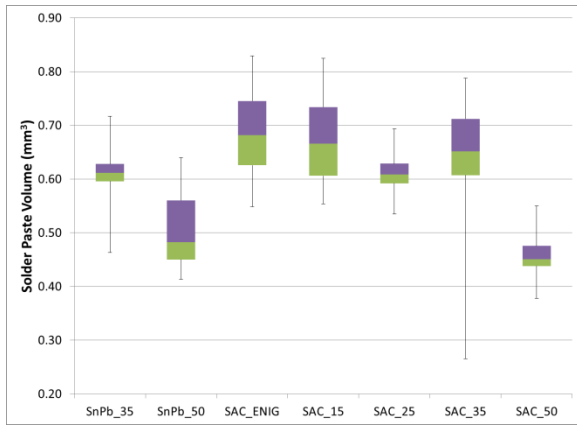Figure 3: Measured solder paste volume under 1206 resistor

Figure 4: Measured solder paste volume under 2512 resistor

The gold content of the solder joints was then computed using the following formulation

$$\frac{l_{bond} \times w_{bond} \times t_{Au} \times \rho_{Au}}{(Vol_{paste} \times Vol\%_{solder} \times \rho_{solder}) + (l_{bond} \times w_{bond} \times t_{Au} \times \rho_{Au})}$$

where l_{bond} and w_{bond} are the solderable length and width of the bond pad, respectively, t_{Au} is the gold plating thickness, ρ_{Au} is the density of gold (19.3 g/cc), vol_{paste} is the solder paste volume, $vol\%_{solder}$ is the metal content in the solder paste, and ρ_{solder} is the density of the solder alloy.

Parametric values and the calculated gold content are displayed in Table 3 and Table 4.

Table 3: Gold Content Calculations for 1206 resistor

Solder	SnPb		SAC305				
Gold Plating Thickness (µm)	1.15	1.42	0.10	0.52	0.75	1.15	1.42
Length Pad (mm)	1.78						
Width of Pad (mm)	1						
Gold Density (g/cc)	19.3						
Solder Paste Volume (cc)	0.3	0.25	0.31	0.31	0.3	0.3	0.23
Paste Metal Content (vol%)	0.5						
Solder Density (g/cc)	8.4	8.4	7.3	7.3	7.3	7.3	7.3
Weight % Gold in Solder	3.0%	4.4%	0.3%	1.6%	2.3%	3.5%	5.5%

Table 4: Gold Content Calculations for 2512 resistor

Solder	SnPb		SAC305				
Gold Plating Thickness (µm)	1.15	1.42	0.1	0.52	0.75	1.15	1.42
Length Pad (mm)	3.76						
Width of Pad (mm)	1.32						
Gold Density (g/cc)	19.3						
Solder Paste Volume (cc)	0.61	0.50	0.69	0.67	0.61	0.66	0.46
Paste Metal Content (vol%)	0.5						
Solder Density (g/cc)	8.4	8.4	7.3	7.3	7.3	7.3	7.3
Weight % Gold in Solder	4.1%	6.0%	0.4%	2.0%	3.1%	4.4%	7.5%

All samples were then aged at 125C for either 0, 168, or 1000 hours. After aging, samples representative of each combination of solder / gold content / aging time were pulled from population and cross-sectioned to observe the morphology of the solder joint and the intermetallic construction and thickness. Sample cross-sectional images are shown in Figure 5 through Figure 9. All electron micrographs were taken at using a LEO 1450 with variable pressure.

The first images are of the baseline SnPb solder samples with the highest percentage of gold content (6.0 wt%) . The observed morphology after 0 hours of aging, seen in Figure 5, is in line with prior studies that show large $AuSn_4$ platelets growing into the Pb-rich phases with high gold content.

After 168 hours of aging at 125C, there is some phase coarsening in the bulk solder, but the $AuSn_4$ intermetallic platelets remain about the same size. At the board-solder interface, a layer of $AuSn_4$ intermetallics, approximately 1.5 microns thick, can to be observed.

After exposure to 125C for 1000 hours at 125C, a significant amount of gold has migrated to the board-solder interface and formed an $AuSn_4$ layer close to 10 microns in thickness. An intermittent layer of Pb-rich phase has formed above the $AuSn_4$ due to the consumption of tin.
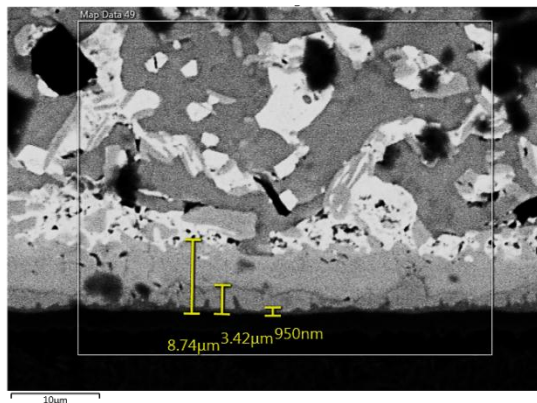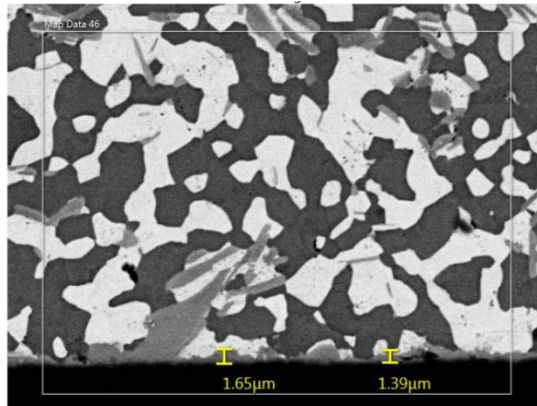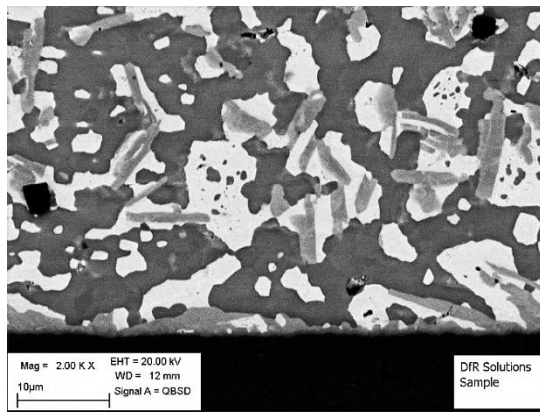
Figure 5 (2000x): Electron micrographs of SnPb Solder with 6.0wt% Gold and Aged for 0 (top), 168 (middle) and 1000 (bottom) hours at 125C

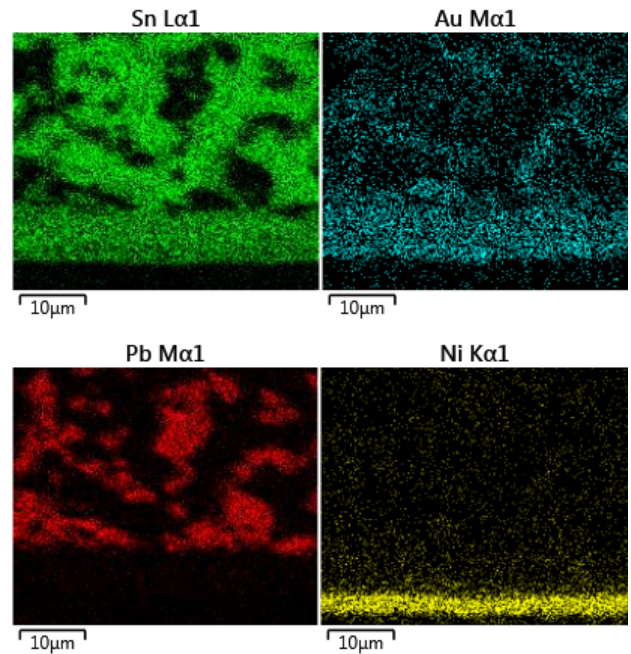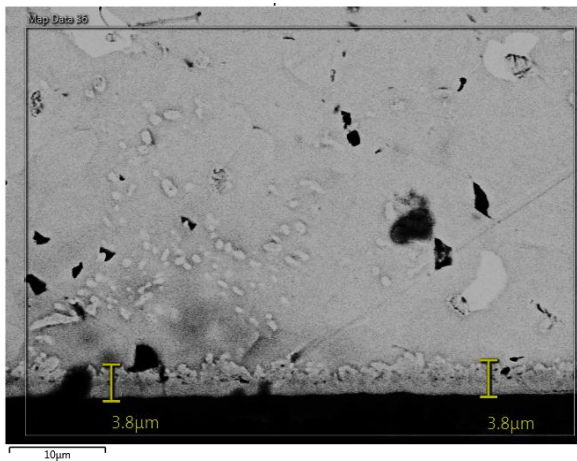An X-ray map of the SnPb solder with 6.0wt% gold and aged for 1000 hours at 125C shown in Figure 6.

Figure 6: Distribution of Sn, Au, Pb, and Ni in SnPb solder with 6.0wt% Gold and Aged for 1000 hrs at 125C

Similar phenomena can be observed with gold content in SAC305 solder. The image of SAC305 solder with 2.0 wt% gold after 0 hours of aging shows a distribution of SnAg and $AuSn_4$ intermetallics in a tin-rich phase. At the board-solder interface, there is a tin-nickel intermetallic layer, approximately 1 to 1.5 microns thick, with sporadic formations of $AuSn_4$.

After aging at 168 hours, the discrete $AuSn_4$ intermetallics at the board-solder interface have increased in thickness, but have not formed a continuous layer. Some coarsening of the SnAg and $AuSn_4$ intermetallics in the bulk solder can also be observed.

After exposure to 125C for 1000 hours, the $AuSn_4$ intermetallics at the board-solder interface have formed a continuous layer. This layer is not uniform and shows extensive variation in thickness compared to the tin-nickel intermetallic layer beneath it. The extent of this layer can be seen in the bottom image in Figure 7 and the X-ray map displayed in Figure 8. The X-ray map also displays an unexpected layer of copper in the area of the $AuSn_4$ intermetallic layer.
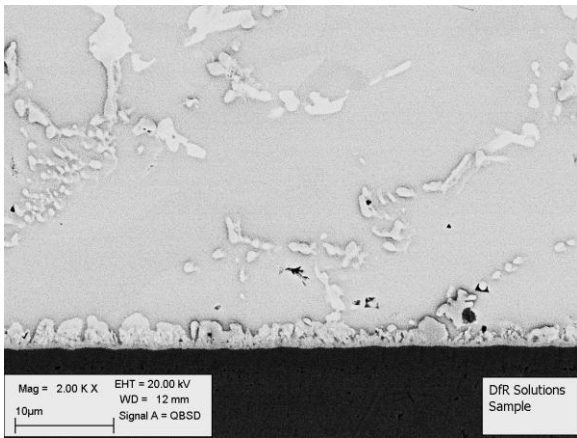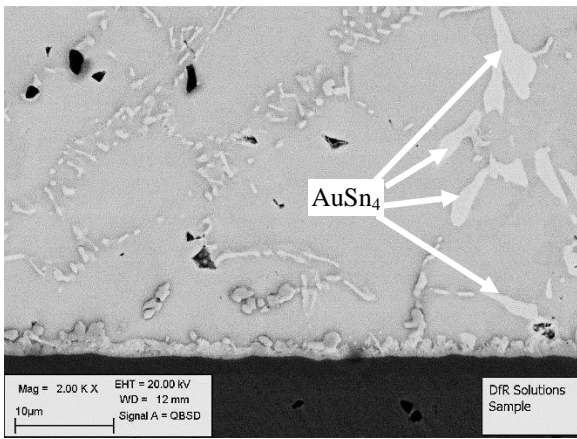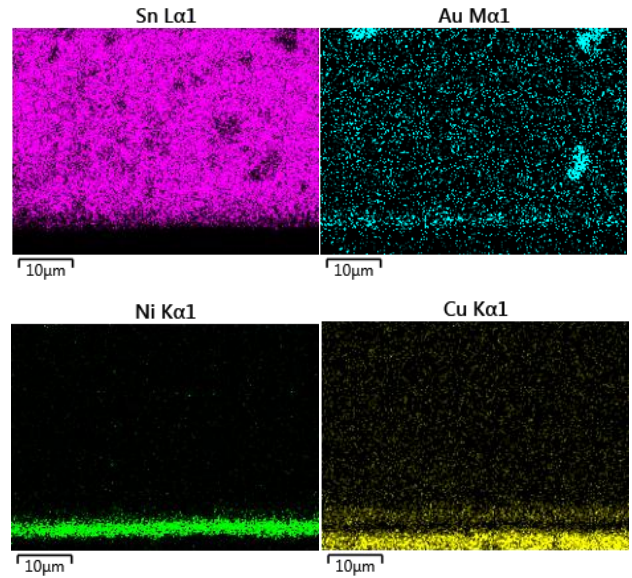
Figure 8: Distribution of Sn, Au, Ni, and Cu in SAC305 Solder with 2.0wt% Gold and Aged for 1000 hours at 125C

Figure 7: Electron micrographs of SAC305 Solder with 2.0wt% Gold and Aged for 0 (top), 168 (middle) and 1000 (bottom) hours at 125C
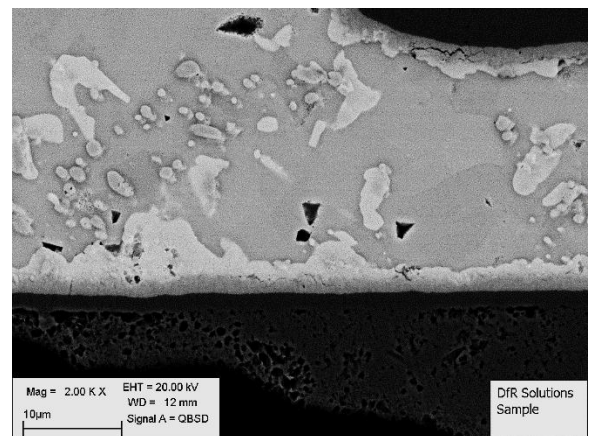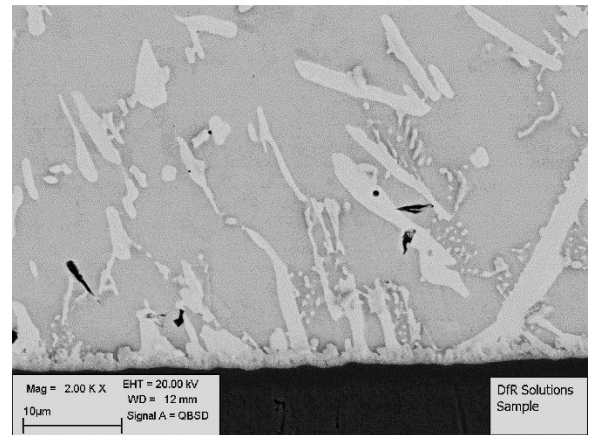

Figure 9: Electron micrographs of SAC305 Solder with 7.5wt% Gold and Aged for 0 (top) and 1000 (bottom) hours at 125C
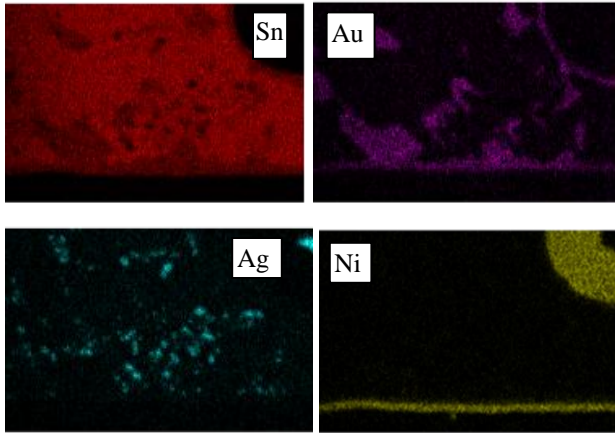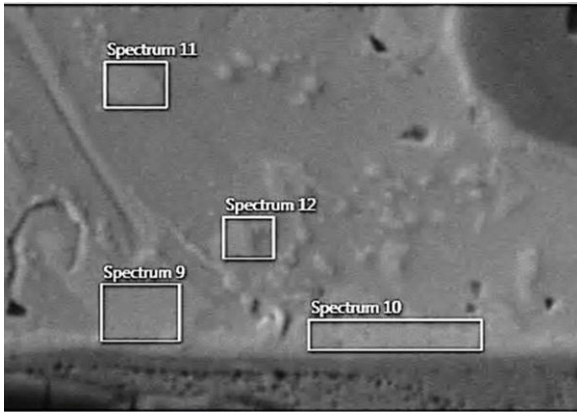
Figure 10: Distribution of Sn, Au, Ag, and Ni in SAC305 with 7.5wt% Gold and Aged for 1000 hours at 125C

After isothermal aging, the remaining samples were subjected to environmental testing, which consisted of either shear testing or temperature cycling.

SHEAR TESTING
Shear test was carried out using a XYZTEC Condor 100. Two types of shear testing were performed: low speed and high speed (impact).

Low Speed Shear Testing
Low speed shear was performed to determine if gold content induced measurable changes in solder strength. The test was performed using the die shear tool at a speed of 2.5 mm/s and a shear height 0.2mm. Shear force measurements were normalized by bond pad dimensions to acquire shear strength values for both 2512 and 1206 resistors. The results as a function of weight percent gold and aging times are displayed in Figure 11 through Figure 13. The dotted green lines are a linear extrapolation of the data.
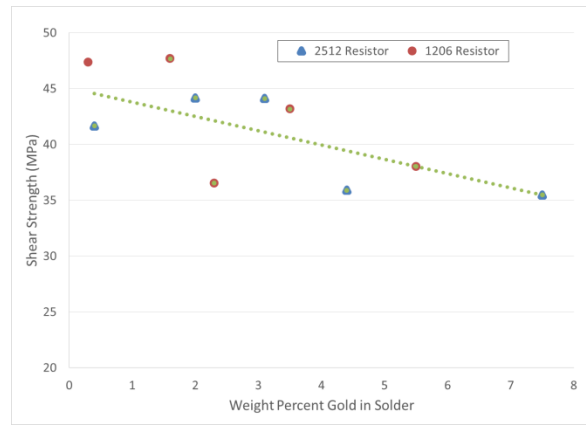

Figure 11: Low Speed Shear Test Results, SAC305 – 0 hr Aging
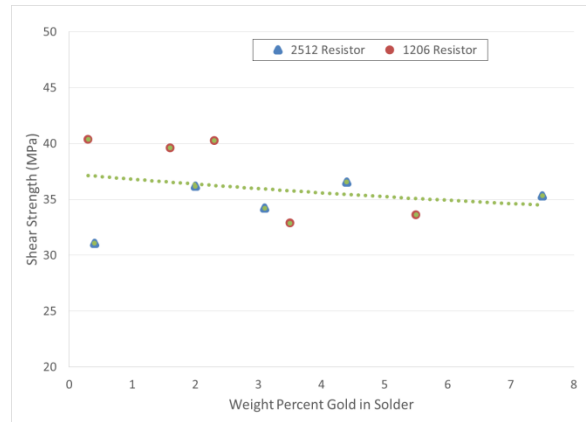

Figure 12: Low Speed Shear Test Results, SAC305 – 168 hr Aging

Figure 13: Low Speed Shear Test Results, SAC305 – 1000 hr Aging

A comparison of the change in solder shear strength as a function of solder alloy is shown in Figure 14. The SnPb samples that are unaged or aged for 168 hours seem to display a substantial drop in shear strength at around four (4) weight percent gold. After 1000 hours of aging, all SnPb samples above three (3) weight percent gold show much lower shear strength. In contrast, the SAC305 samples seem to show a gradual reduction in strength as a

function of weight percent gold, with no defined transition from high to low shear strength.
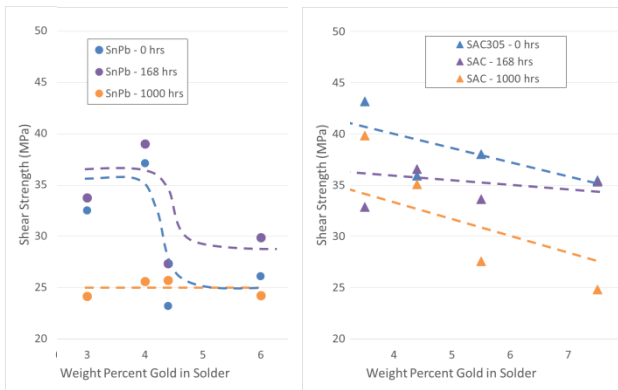

Figure 14: Low Speed Shear Test Results – SnPb (left) and SAC305 (right)

High Speed Shear Testing
High speed shear testing was performed to determine if impact speed would show a greater differentiation between gold content and aging times. The test was performed using the high speed impact tool at a speed of 800 mm/s and a shear height 0.1mm. Given the load limitations of the impact tester, only the 1206 resistors were tested.

A variety of techniques were used to post process the data from the high speed testing to compensate for different failure modes. The energy that just captures the first fracture (first peak) is shown in Figure 15. The total energy dissipated during the impact results are shown in Figure 16. The dashed lines are linear extrapolations of the results.
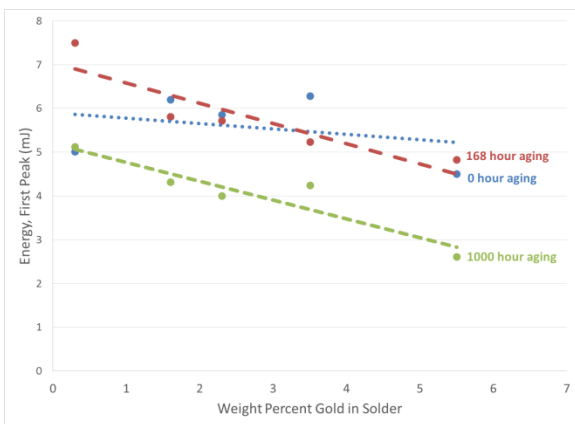

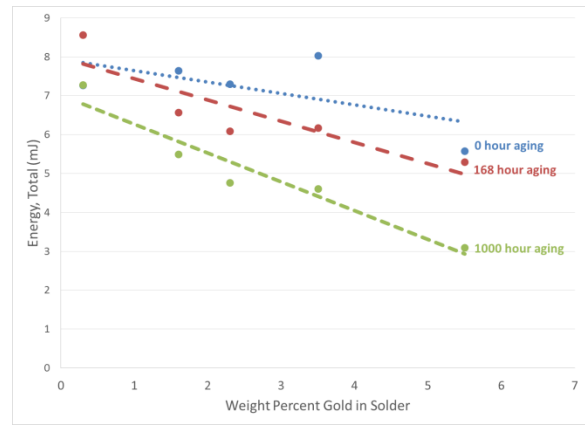Figure 15: High Speed Shear Test Results, SAC305 – First Peak Energy

Figure 16: High Speed Shear Test Results, SAC305 – Total Energy

A comparison of change in impact energy as a function of solder alloy is shown in Figure 17 and Figure 18.
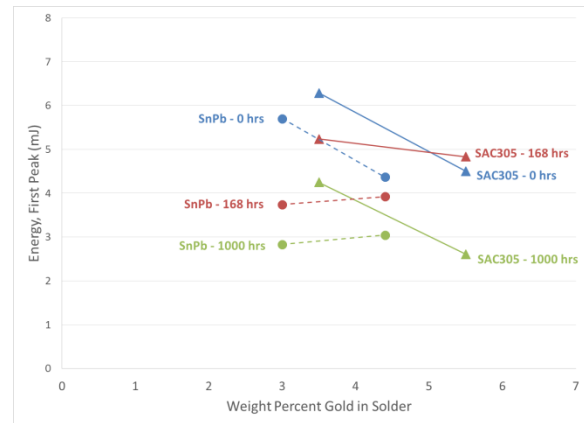

Figure 17: High Speed Shear Test Results, SnPb and SAC305 – First Peak Energy

Figure 18: High Speed Shear Test Results, SnPb and SAC305 – Total Energy

High Speed Shear Testing – Fracture Surfaces
After high speed (impact) testing, fracture surfaces were examined to assess the degree of ductile and brittle fracture. Representative images of these fracture surfaces are displayed in Figure 19 through Figure 23.

For SnPb solder with 4.4wt% gold and no aging, seen in Figure 19, the failure can be seen to be ductile in nature and the fracture surface propagates through the bulk solder. A similar behavior is seen after 168 hours of aging, also seen in Figure 19.
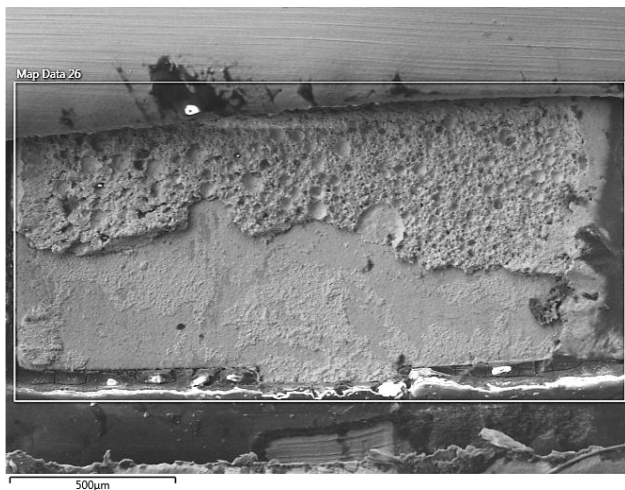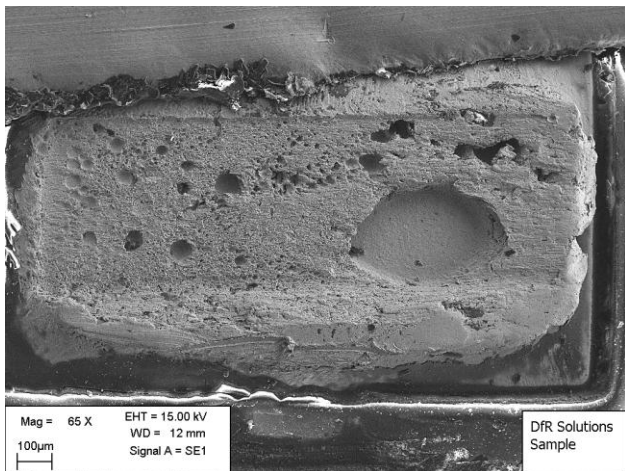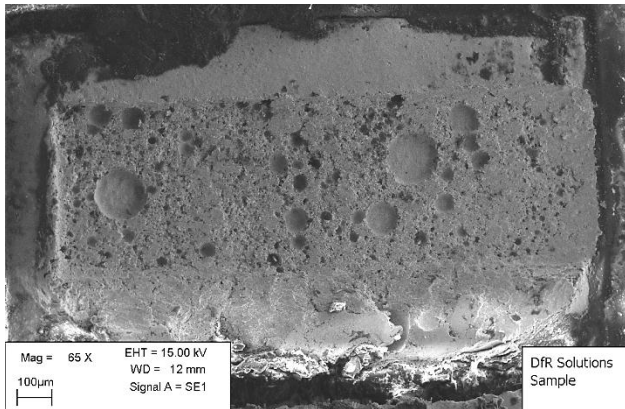

Figure 19: High Speed (Impact) Fracture Surfaces of SnPb Solder with 4.4wt% Gold and Aged for 0 (top), 168 (middle), and 1000 (bottom) hours at 125C
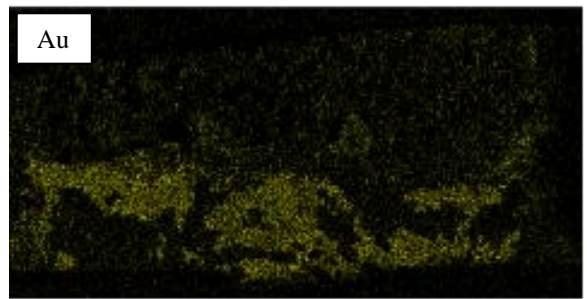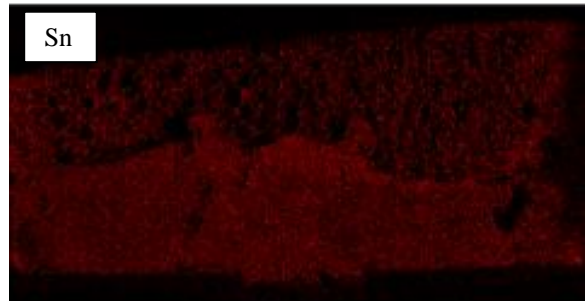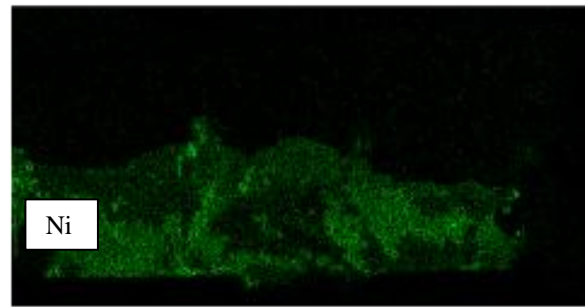

Figure 20: Elemental map of SnPb solder with 4.4wt% Gold and Aged for 1000 hrs at 125C

Once aging times increase to 1000 hours, we see the transition from ductile to brittle failure. The lower portion of the fracture surface in Figure 19 / bottom shows a smoother surface, suggesting fracture at an intermetallic layer. This is confirmed through elemental mapping (see Figure 21), which shows the crack alternating between the interface between the SnNi and $AuSn_4$ intermetallic layers and the interface between the $AuSn_4$ intermetallic and the bulk SnPb solder.

SAC305 solder with 1.6wt% displays ductile behavior for all three aging conditions. This is confirmed through the X-ray map displayed in Figure 22, which reveals a fracture surface dominated by tin (Sn), with trace amounts

of nickel (Ni), gold (Au), and silver (Ag). These results are expected for fracture through the bulk solder.
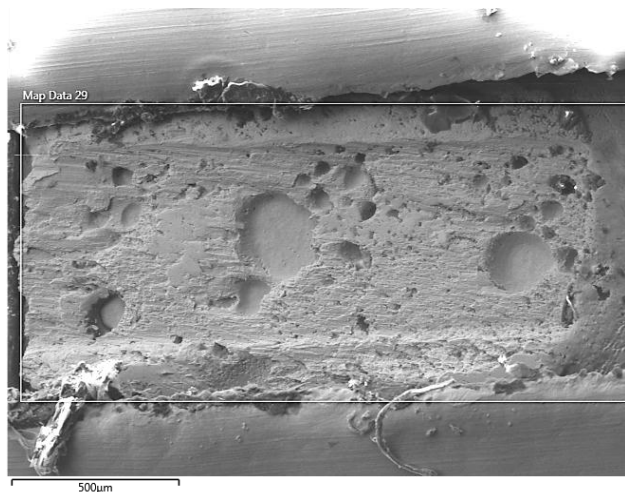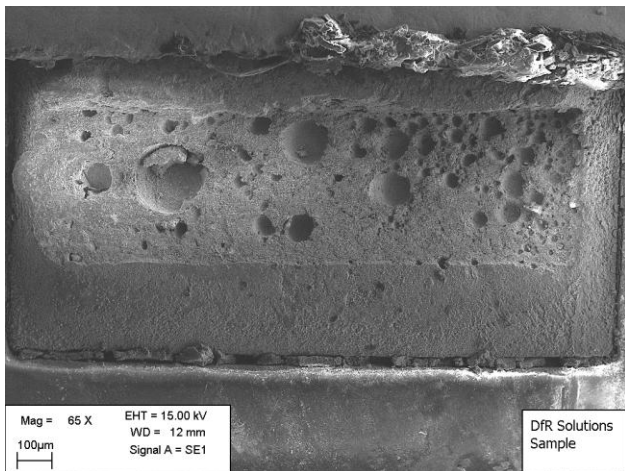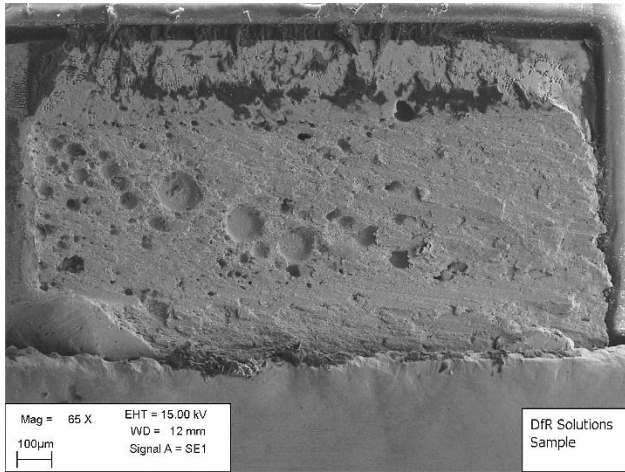

Figure 21: High Speed (Impact) Fracture Surfaces of SAC305 Solder with 1.6wt% Gold and Aged for 0 (top), 168 (middle) and 1000 (bottom) hours at 125C
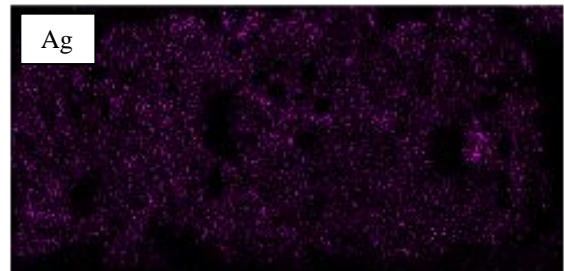

Figure 22: Elemental map of SAC305 solder with 1.6wt% Gold and Aged for 1000 hrs at 125C

For SAC305 solder with higher amounts of gold (5.5wt%) and 0 hours aging, seen in Figure 23, the failure is ductile in nature and the fracture surface propagates through the bulk solder. A similar behavior is observed after 168 hours of aging.

After 1000 hours of aging, the fracture behavior has transitioned to a brittle mechanism. The fracture surface is smoother when compared to 0 and 168 hours of aging.

Reviewing the elemental maps in Figure 24, the crack path is seen to have primarily propagated between the $AuSn_4$ and the SnNi intermetallic layers. In some areas, crack seems to have deviated into the interface between the SnNi intermetallic and the underlying nickel plating.
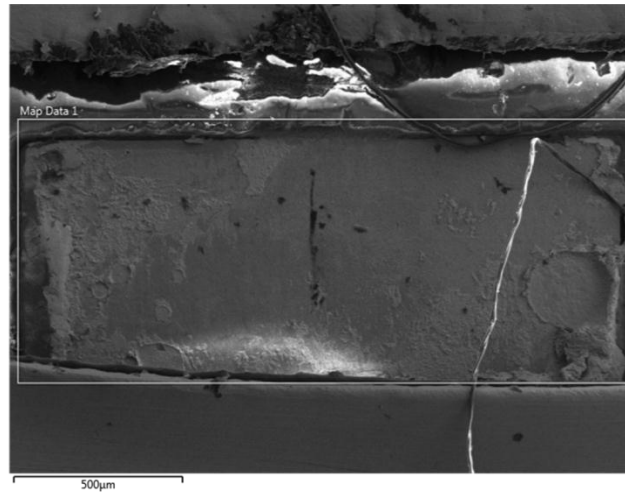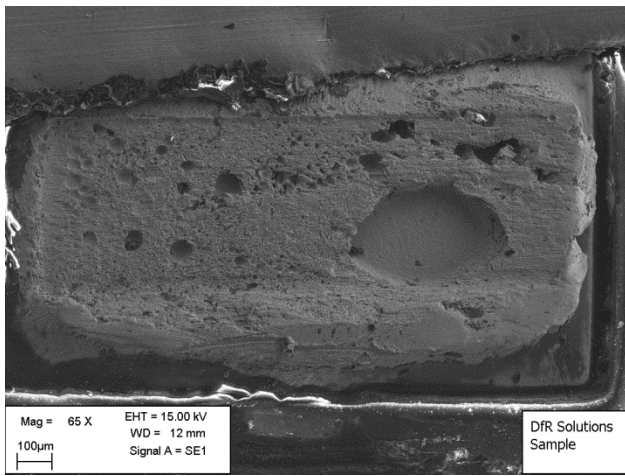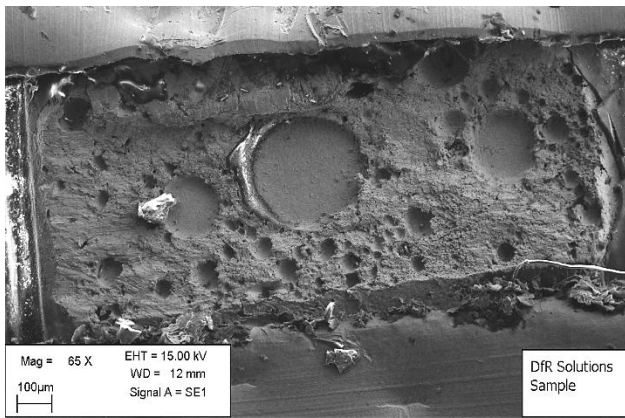
Figure 23: High Speed (Impact) Fracture Surfaces of SAC305 Solder with 5.5wt% Gold and Aged for 0 (top) and 1000 (bottom) hours at 125C
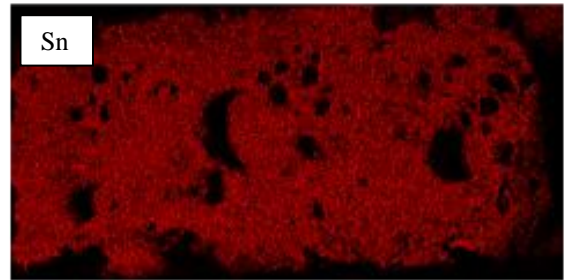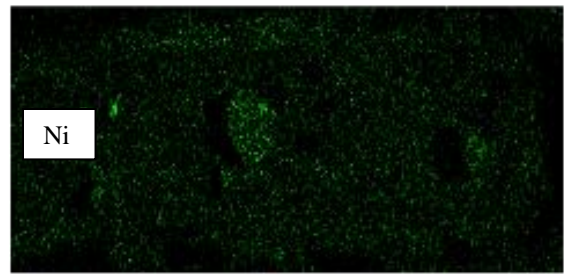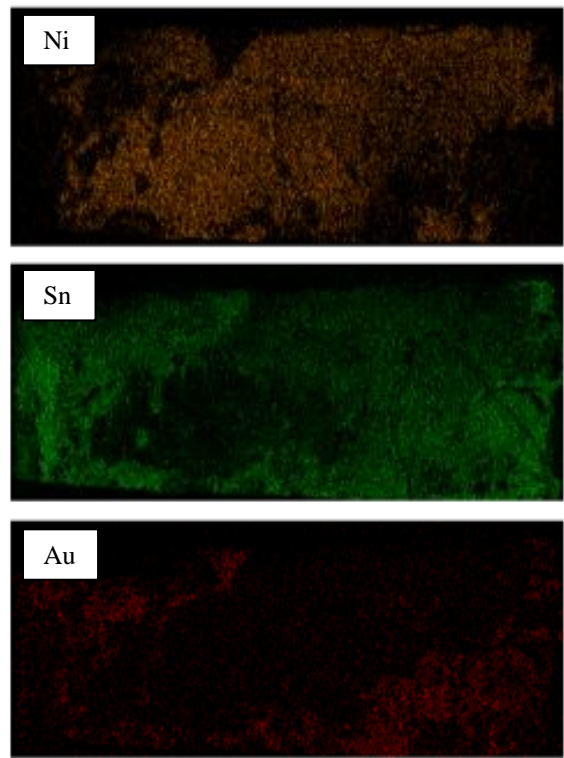

Figure 24: Elemental map of SAC305 solder with 5.5wt% Gold and Aged for 1000 hrs at 125C

THERMAL CYCLING

Test boards were thermal cycled from 0 to 100°C with 10 minute dwells and 5 minute ramps. Samples were subjected to up to 4500 temperature cycles depending upon aging times.

Resistance was monitored using an Agilent 34970A Data Acquisition Switch Unit with three (3) 40 channel single-ended multiplexer modules. Resistance was captured every 70 seconds. Nominal resistance was approximately one (1) to two (ohms) as seen in Figure 25.
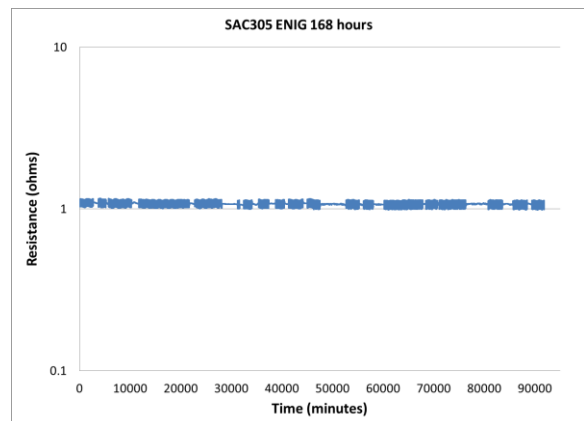
Figure 25: Resistance vs. Time, Thermal Cycling of SAC305 with 0.4% Gold and Aged for 168 hours at 125C

To minimize false detection error, the failure criteria was defined as when resistance increased by 10 times (10X) the range of variation in resistance [7]. Using this approach avoided false detection errors and response to variations driven by channels, wiring, and board level connections. Examples of the resistance variation are shown in Figure 26 and Figure 27.

Figure 26: Resistance vs. Time, Thermal Cycling of SnPb with 6.0% Gold and Aged for 1000 hours at 125C

Figure 27: Resistance vs. Time, Thermal Cycling of SAC305 with 3.1% Gold and Aged for 1000 hours at 125C

Failure data was then gathered and fitted to two-parameter Weibull distributions. The Weibull parameters are listed in Table 5. The 1000 hour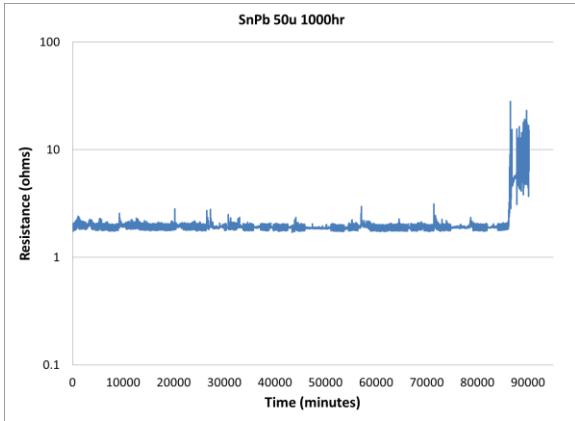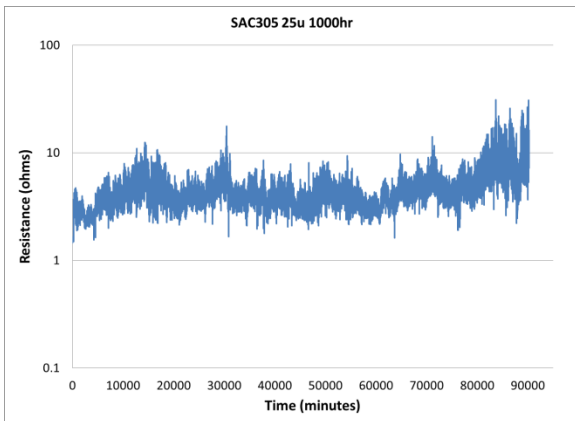 aged samples tended to not experience failure because they were subjected to fewer temperature cycles (2757 cycles) then the 168 hour aged samples (4724 cycles).

Table 5: Thermal cycling results for 2512 resistors, Weibull parameters

Alloy	Gold Wt %	Aging (hours)	Characteristic Life, η	Slope β	Total Cycles
SnPb	4.1%	168	4950	3.1	4724
SnPb	6.0%	168	3112	4.3	4724
SnPb	4.1%	1000	No Failures		2757
SnPb	6.0%	1000	2441	9.8	2757
SAC305	0.4%	168	No Failures		4724
SAC305	2.0%	168	5382	6.2	4724
SAC305	3.1%	168	4235	5.9	4724
SAC305	7.5%	168	2705	6.1	4724
SAC305	0.4%	1000	No Failures		2757
SAC305	2.0%	1000	No Failures		2757
SAC305	3.1%	1000	No Failures		2757
SAC305	4.4%	1000	No Failures		2757
SAC305	7.5%	1000	3209	2.5	2757

A Weibull plot of thermal cycling failures as a function of gold content, after 168 hours of aging, is shown in Figure 28. There seems to be a strong influence of gold content, with increasing gold content resulting in measurable reduction in time to failure.

Weibull plots showing the influence of aging time (168 vs. 1000 hours) and solder alloy (SAC305 vs. SnPb) are shown in Figure 29 and Figure 30.
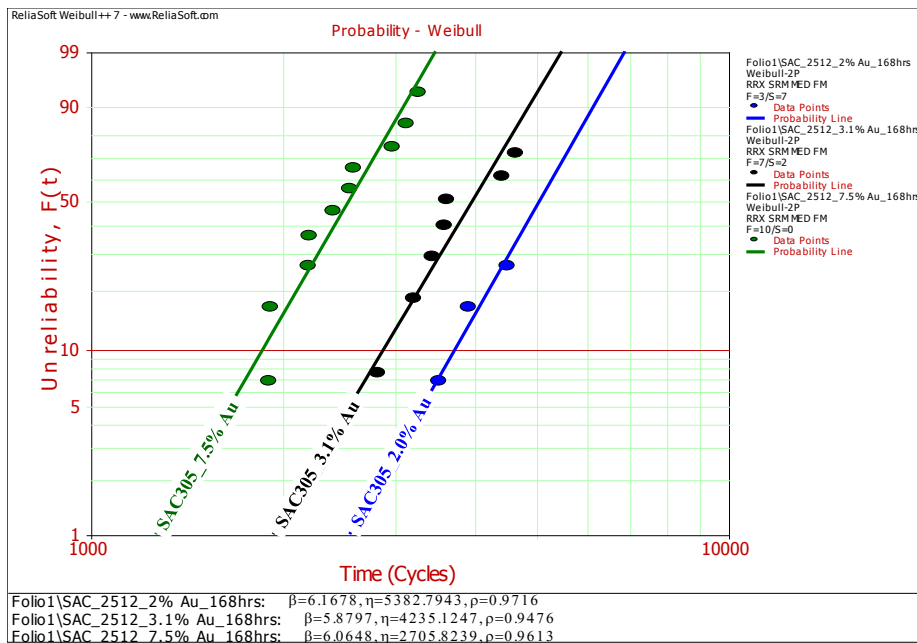
Figure 28: Weibull plots of thermal cycling failures (0 to 100C) as a function of gold content (2512 Resistors, Aged for 168 hours at 125C)
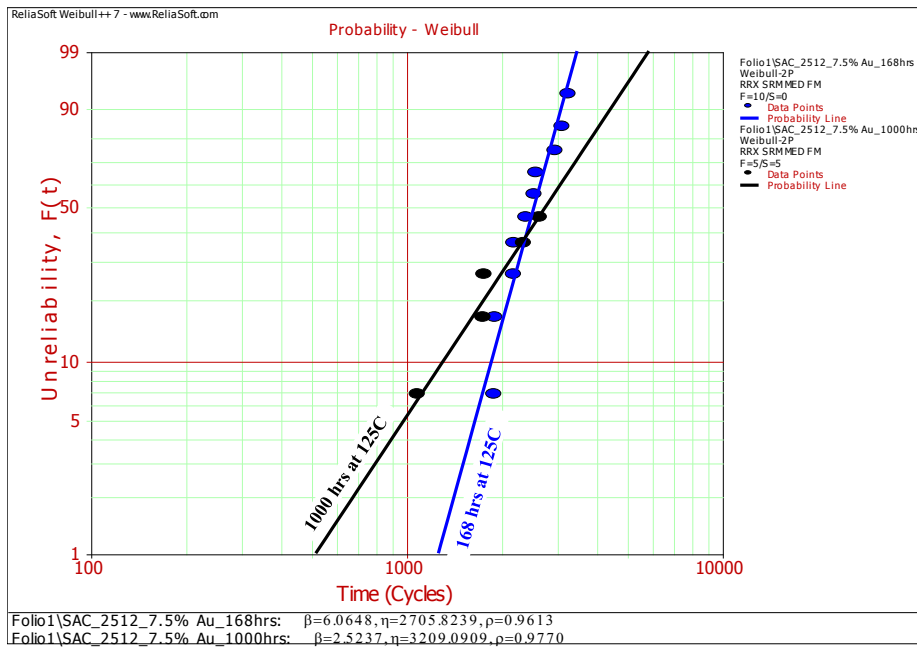

Figure 29: Weibull plots of thermal cycling failures (0 to 100C) as a function of aging time (2512 Resistors, SAC305 with 7.5% Gold)
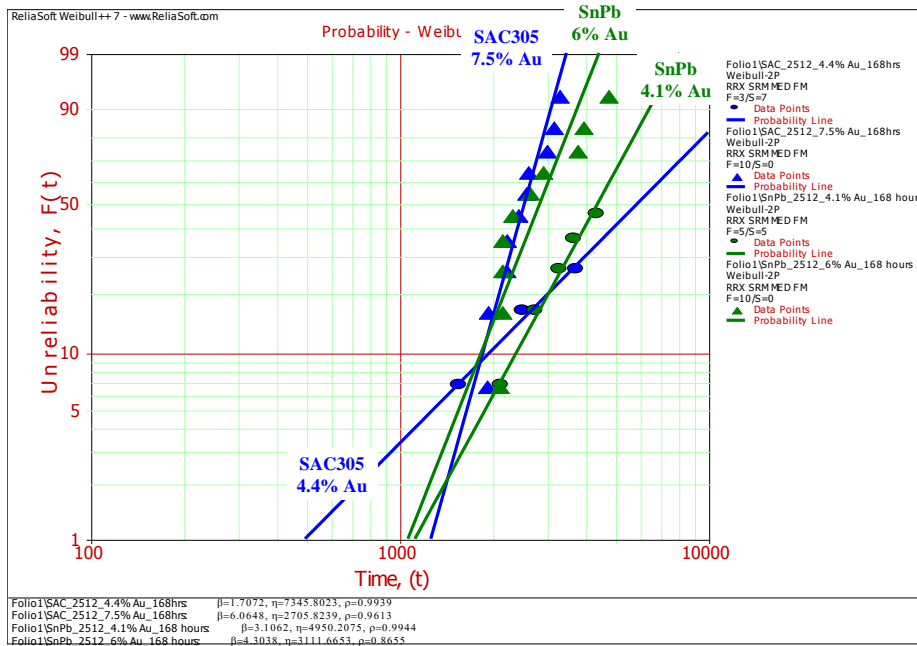
Figure 30: Weibull plots of thermal cycling failures as a function of solder alloy (2512 Resistors, Aged for 168 hours at 125C)

A plot of time to failure under temperature cycling as a function of gold content can be seen in Figure 31. All samples in Figure 31 were aged for 168 hours. A clear trend can be observed, with increasing gold content decreasing characteristic lifetimes by approximately 500 cycles / 1% Au for SAC305 solder.
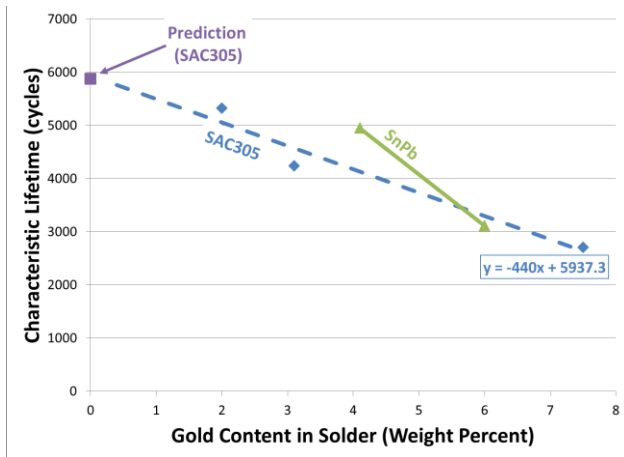

Figure 31

DISCUSSION
The results of shear testing and temperature cycling demonstrate a degradation in SAC305 properties with increasing gold content. Observation of changes in morphology of the solder joint and different trending for mechanical and thermal testing suggest two different mechanisms play a role in this behavior.

After the initial rapid dissolution of gold into the molten SAC305 solder, the insoluble nature of gold into tin drives the formation for $AuSn_4$ intermetallics. These intermetallics are initially randomly distributed throughout the bulk solder (see Figure 5). As aging at elevated temperature occurs, the Au diffuses toward the Ni_3Sn_4 intermetallic layer, forming a $(Au,Ni)Sn_4$ phase []. It is believed that the driving force for this migration is a reduction in free energy []. As seen in Figure 10, this occurs when Ni_3Sn_4 is present at both the board and component interfaces.

The selective introduction of harder intermetallic reinforcements is a well-known technique for improving the strength and temperature cycling performance of tin-based alloys [12]. As shown in this study, the presence of $AuSn_4$ intermetallics results in a decrease in strength and thermal cycling performance. For samples that were unaged or aged for a limited period of time, this degradation is driven by the overall size of the $AuSn_4$ intermetallics. Larger intermetallic needles or platelets can fracture more easily under mechanical loads, creating stress concentrations that accelerate crack propagation [13].

This expectation of early fracture is especially true for $AuSn_4$ compared to Ag_3Sn due to the larger size of the $AuSn_4$ phase and the higher maximum modulus (131 GPa [13] vs. 94 GPa [15])(the anisotropic structure of $AuSn_4$ and Ag_3Sn crystal results in different moduli in different crystallographic orientations)(there is significant debate regarding the true modulus of $AuSn_4$, with some papers presenting values as low as 39 GPa [16]; the authors

chose value from reference [13] because of its basis on first principles)

Early fracture of intermetallic particles in the bulk solder provides some explanation of the reduction in shear strength and impact energy with increasing gold content. This is especially true for shear and impact test failures that occurred in the bulk solder.

The interface between the intermetallic and the bulk solder can also be a source of weakness depending upon the characteristics of the interfacial bonding. While there is little numerical data in the literature on the strength of interfacial bond between $AuSn_4$ and β-Sn, prior studies have indicated a weak interface between $AuSn_4$ and SnPb [17] and X-ray maps of surfaces after impact testing demonstrate that crack propagation can occur between $AuSn_4/(Au,Ni)Sn_4$ and β-Sn. The buildup of a gold-containing layer at the interface, either due to the amount of gold present within the solder or diffusion of gold over time at elevated temperatures, in combination with a weak interface would decrease the strength of the solder joint.

It is this duality of failure locations, fracture of the intermetallic in the bulk and separation along a gold-rich layer at the interface, that may explain the shear strength trends observed in Figure 11 through Figure 13. Shear strengths at time zero are dominated by the amount of $AuSn_4$ within the bulk SAC305 solder. Initial aging of the SAC305 solder allows the gold in the immediate vicinity of the interface to diffuse towards the SnNi intermetallic. This migration weakens the interface and the surrounding solder (discussed as a denuded region in the paragraph below). For SAC305 solder with low gold content, the interfacial region becomes the weak link. For SAC305 with high gold content, the bulk solder with fractured $SnAu_4$ intermetallics remains the failure site.

With longer term aging, the amount of gold available in low gold content SAC305 solder is limited. With higher amounts of gold, the $(Au,Ni)Sn_4$ layer continues to increase in thickness and becomes more uniform (less scalloped) further reducing the interfacial strength.

Large intermetallics can also introduce denuded regions adjacent to the platelet/ whisker, where the matrix is significantly softer [13]. This can promote strain localization, accelerating plastic and creep driven damage that is known to accelerate thermomechanical fatigue. This denuded region may also be a failure site during shear and impact testing, where the bulk solder directly adjacent to the $(Au,Ni)Sn_4$ intermetallic is weaker. This weakness within the bulk solder could contribute to a reduction in shear strength and impact energy without inducing brittle failure at the intermetallic. This has been observed in SnPb solder, where the reaction of Sn to either gold or nickel can create Pb-rich regions that are inherently weaker than the SnPb matrix.

These three processes, intermetallic fracture, interfacial strength, and denuded regions, likely all play some role in the degradation of SAC305 with increasing gold content and increasing aging time. Of additional interest is the continuous rate of that degradation. Unlike the SnPb solder samples, which demonstrated a sharp drop in shear strength at around 4 weight percent gold (in line with the historical guidelines of no more than 3 weight percent gold), the properties of SAC305 degrade progressively for all three test conditions (shear, impact, and thermal cycling).

CONCLUSION
In shear testing, impact testing, and thermal cycling, SAC305 solder joints degrade with increasing gold content. There does not appear to be a threshold between "good" and "bad". While the results indicate that SAC305 joints have higher strength than SnPb solder joints at similar gold content and age, we cannot recommend a limit on the weight percent of Au in SAC305 solder joints.

Specific findings from this study include
1) Both low speed shear test and high speed impact test show that the shear strength of SAC305 solder joints decreases as the gold content increases. The degradation in shear strength and impact accelerates with aging.
2) Ductile to brittle transition in SAC305 seemed to occur when the total energy dissipated during impact testing was less than 4 mJ. When brittle fracture occurs, the primary crack path is between the $AuSn_4$ and SnNi intermetallics.
3) The embrittlement of SAC305 solder is driven by the precipitation of a $AuSn_4$ intermetallic layer between the bulk solder and the SnNi intermetallic. This failure mode is similar to behavior observed in SnPb solder with elevated levels of gold.
4) Increasing gold content has deleterious effects on thermal cycling performance of SAC305 solder joints.
5) Unlike SnPb solder, the embrittlement and degradation of SAC305 solder due to increasing gold content seems to more progressive than abrupt.

REFERENCES
1. Gordon Foster, Embrittlement of Solder by Gold from Plated Surfaces, ASTM STP319 / STP45806S, pp. 13-19, Jan. 1963
2. W.B. Harding and H.B. Pressly, `Soldering to gold plating', Am. Electroplat. Soc., 50th Annu. Proc., 1963, 90-106
3. M.H. Bester, `Metallurgical aspects of soldering gold and gold plating', Proc. Inter/Nepcon, 1968, Brighton, Chicago 1969, 211-31
4. R.N. Wild, `Effects of gold on the properties of solders', IBM Federal Systems Div, Owego, Rep. No. 67-825-2157, Jan. 1968

5. J. Glazer, P.A. Kramer, and J.W. Morris, Jr. (1992), "Effect of Gold on the Reliability of Fine Pitch Surface Mount Solder Joints," Circuit World, Vol. 18, No. 4, pp. 41-47.

6. Banks, Sherman. "Reflow soldering to gold." Electronic Packaging and Production (1995): 69.

7. Hernandez, C. L., Vianco, P. T. and Rejent, J. A., "Effect of interface microstructure on the mechanical on the mechanical properties of Pb-free hybrid microcircuit solder joints", Proceedings, IPC / SMTA Electronics Assembly Expo, October 27-29, 1998, Providence, RI, pp. S19-1-1 to S19-1-8.

8. Jianbiao Pan; Silk, J.; Powers, M.; Hyland, P., "Effect of Gold Content on the Reliability of SnAgCu Solder Joints," Components, Packaging and Manufacturing Technology, IEEE Transactions on , vol.1, no.10, pp.1662,1669, Oct. 2011

9. Mike Powers, Jianbiao Pan, Julie Silk, Patrick Hyland, Effect of Gold Content on the Microstructural Evolution of SAC305 Solder Joints Under Isothermal Aging, Journal of Electronic Materials, February 2012, Volume 41, Issue 2, pp 224-231

10. Nausha Asrar, Detrimental Effects of Excessive Gold Plating on Lead-Free Solder Joints, Journal of Failure Analysis and Prevention, February 2010, Volume 10, Issue 1, pp 50-55

11. J. Pan, J. Silk, 'A Study of Solder Joint Failure Criteria,' 44th Inter. Symp. Microelectronics, Oct. 9-13, 2011, Long Beach, CA.

12. Dudek, R.; Faust, W.; Wiese, S.; Rollig, M.; Michel, B., "Low-cycle Fatigue of Ag-Based Solders Dependent on Alloying Composition and Thermal Cycle Conditions," Electronics Packaging Technology Conference, 2007. EPTC 2007. 9th , vol., no., pp.14,20, 10-12 Dec. 2007

13. J. P. Lucas, H. Rhee, F. Guo, K. N. Subramanian, 'Mechanical properties of intermetallic compounds associated with Pb-free solder joints using nanoindentation', Journal of Electronic Materials, 2003, Volume 32, Issue 12, pp 1375-1383

14. Rong An; Chunqing Wang; Yanhong Tian, "Depiction of the elastic anisotropy of AuSn4 and AuSn2 from first-principles calculations," Electronic Packaging Technology & High Density Packaging, 2009. ICEPT-HDP '09. International Conference on , vol., no., pp.611,616, 10-13 Aug. 2009

15. N.T.S. Lee, V.B.C. Tan, K.M. Lim, "Structural and mechanical properties of Sn-based intermetallics from ab initio calculations," Appl. Phys. Lett. 89 (2006)

16. R.R. Chromik, D-N. Wang, A. Shugar, L. Limata, M.R. Notis and R.P. Vinci, 'Mechanical Properties of Intermetallic Compounds in the Au–Sn System'. Journal of Materials Research, 20, pp 2161-2172 (2005).

17. David M. Jacobson, Giles Humpston, 'Gold coatings for fluxless soldering,' Gold Bulletin, March 1989, Volume 22, Issue 1, pp 9-18, 1989